Strathprints Institutional Repository

Surface engineering of Ti-6Al-4V by nitriding and powder alloying using a CW CO_2 laser.

T. N. Baker [1] and M. S. Selamat [2]

1 Metallurgy and Engineering Materials Group, Department of Mechanical Engineering University of Strathclyde, Glasgow G1 1XN, U.K.

2 Formerly, Metallurgy and Engineering Materials Group, Department of Mechanical Engineering University of Strathclyde, Glasgow G1 1XN, U.K.

Now, Advanced Materials Research Centre (AMREC), SIRIM Berhad

Persiaran Dato Menteri, P. O. Box 7035, Section 2

40911 Shah Alam, Malaysia.

Corresponding author: Professor T.N.Baker, Metallurgy and Engineering Materials Group, Department of Mechanical Engineering, University of Strathclyde, Glasgow G1 1XN, U.K.

Phone: 01415483101, Fax: 01415525105, e-mail; neville.baker@strath.ac.uk

ABSTRACT

A comparison has been made of the laser processing of Ti-6Al-4V (IMI-318) alloy by (a) nitriding under a dilute atmosphere, (b) preplaced 6 μm SiC powder and (c) a combination of (a) and (b). At least six laser tracks were overlapped. Microhardness maps allowed details of the variation in hardness with both melt depth and track number to be determined. The microstructure was characterised and related to the processing parameters, melt track dimensions, hardness and roughness data.

It was found that the preheat generated due to the overlapping, influenced the individual track dimensions, microstructure and properties, which were also affected by the laser energy density and the nitrogen concentration in the nitriding atmosphere used in processing. Process (b) was shown to produce the smoothest surfaces, with R_a values <2μm, whilst (c) gave the highest R_a, value, 8.6 μm. These results are considered together with a wide range of data in the literature on laser processed Ti-6Al-4V.

Introduction

For over 25 years, laser surface engineering techniques involving the subsequent rapid solidification of the molten surface have been used to improve the wear, corrosion and erosion resistance of titanium alloys, which are known to display poor tribological properties such as a high coefficient of friction, difficulties in lubrication, and low adhesive and fretting wear resistance[1].Methods of enhancing these surfaces properties of titanium alloys by nitriding and other means have recently been reviewed [2,3]. Despite the relative maturity of the laser surface engineering of titanium alloys, research leading to an improvement in the surface properties is very active worldwide as shown by the number of papers published in recent years. While the laser alloying of titanium alloys through nitriding has been studied extensively, for example [4-16], the original approach used powder injection methods, and it is in this area that most activity is now found. The early work was based on TiC[17,18], WC [17,18] and SiC [19] powders of around 150μm in size. In more recent work, this average size was reduced to particles within the range 60-100μm [20-23]. An alternative method is the preplacement of particles on the surface of the substrate alloy in the form of a slurry, where in general, the particles have a smaller average size, ~ 45-60 μm [24, 25]. Both these techniques result in the partial dissolution of the particles which can provide a strong bond between the particle and the matrix, and confer significant wear resistance to the substrate[14, 18,24, 25]. However, for some applications which require improved surface strength through dispersion hardening and /or improved corrosion properties, a complete dissolution of the powder particles during laser processing is beneficial. This is possible using laser powers of ~3kW, when the particle size is less than 10μm .Using SiC particles, both of these techniques provided an opportunity for the precipitation, in a fine state, of new phases, Ti_5Si_3 and TiC [24, 26-29].It is generally found that the hardness of the powder alloyed surface is lower than that of the

nitrided specimens. Other elements and compounds that have been incorporated into titanium alloys include, Al [30-34], B_4C [35], BN [36], Si [34,36], TiC [17,18,37-40], TiN [14,24,41], ZrC [24] and ZrN [24]. Mixed alloy powders such as Al+ Si [34,37], Mo-WC [23],Ti-Cr_3C_2 [40], and Ti-TiB [42] have also been studied, as have complex powders which include BN-NiCrCoAlY [43], NiCrBSiC [44,45], NiCrBSi-TiC [38],NiCrBSiC-TiC [37,39,45], Ti_5Si_3+$NiTi_2$ [46] and $Zr_{65}Al_{7.5}Ni_{10}Cu_{17.5}$ [47].Laser alloying with graphite[48], graphite and silicon mixed powders [49], graphite, boron and RE oxides [50], and nitrogen and carbon separately [51], has been undertaken. The combination of powders with gaseous atmospheres has also been studied; in particular mixtures of nitrogen with SiC [24,28,29,52,53] ,TiN [14], ZrC [14] and with ZrN [24]. The combination of dilute nitrogen atmospheres and powder alloying has been found to produce crack- free surfaces which have additional hardness relative to the titanium parent alloy and the powder alloying alone [27-29, 52-55].

While many of these studies reported a significant increase in the hardness of the alloyed layer relative to the substrate, very few commented on the soundness of the material following laser processing. The early work using laser gas nitriding reported cracking in the alloyed layer.[6, 8,20, 56,57]. Other defects recorded included porosity and segregation bands arising from convective Maragoni forces[9].It is also the case that most publications describe work which produced either a small hemispherical volume of modified surface or a single laser track with a width of a few millimeters, running the length of the specimen. In practice, there is frequently a requirement to produce an MMC coating over a much greater surface area. This necessitates the overlapping of many laser melted tracks with the additional problems of preheating of the regions of the substrate where subsequent tracks are to be placed [20, 56]. Furthermore, due to the influence of the preheat on the microstructure, characterisation of the microstructure of a single track, usually unidentified, may not be representative of the variations which occur between the first

and subsequent tracks, and possibly give misleading information. The same criticism can be made of the way in which, normally, single indents are used to follow the change in hardness with depth through the laser processed surface. When overlapping tracks are made, it is preferable to follow changes in hardness by creating a microhardness map using a low load of 30-100g, to reveal local variations in hardness. In particular, the variation in the phases identified in single track experiments with those formed within different tracks following multi- track processing has received virtually no attention, and neither has the variation in the phases formed at different melt depths in the melt zone[20,56]. Another important factor is the depth of surface after a laser treatment which is to be removed prior to a final treatment, such as shot peening, a treatment used in part to produce a compressive stress as a means of improving fatigue life..

The present work compares three methods of laser surface engineering a Ti-6Al-4V alloy through (a) laser nitriding (b) powder alloying with SiC and (c) a combination of laser nitriding and SiC powder alloying. The results are considered together with data available in the literature, including that which has been obtained with a variety of powder alloying systems to accomplish laser surface engineering. This will be used to establish if any one approach has a significant advantage in developing an optimum laser processed surface layer.

Experimental techniques

Commercial Ti-6Al-4V (IMI-318) supplied by Imperial Metals Industries, U. K., was used as the base alloy in the present study. The composition of the alloy in wt% was <0.08%C, <0.25%Fe, <0.05%N, <0.2%O, <0.015%H, 5.5-6.75%Al, 3.5-4.5%V and Ti (balance). Base alloy specimens, coded A,B, and C, of size 100mm x 100mm and 10mm thickness were cut from the as-received material for laser processing. The specimens were abraded with 600 grit SiC papers, and then cleaned with methanol. The abraded

surfaces avoided high energy reflection during laser treatment. SEM observations confirmed that the SiC particles were not embedded as a result of the abrasion. Two of the specimens, coded B and C, were coated with SiC particles, of average size 6μm, which were blended with an organic binder and painted on the surface of the base alloys[26,29,57]. For all three specimens, a spinning beam mode [29,54,58] was produced by a continuous wave CO_2 laser to give an~ 2mm wide melt track using a velocity of spinning of 1500 r.p.m. 50% overlaps were made for all three specimen groups. The nitrogen and argon gas flow rate for all the laser processing was 10 l/min.

Laser nitriding was carried out on specimen A[13, 58, 59] with a 20% nitrogen and 80% argon environment. The laser power was set at 3 kW, the specimen velocity was 3mm/s and a total of 12 laser overlapping tracks was produced.

The laser surface alloying of specimen B [13, 29] was carried out in a 100% argon environment, with 6μm SiC powder preplaced on the alloy. A total of 6 laser tracks were melted.

In the case of specimen C, processing was undertaken using a combination of a 40% nitrogen and 60% argon environment together with preplaced SiC powder[52-54]. As the nitrogen has to diffuse through the powder before reacting with the melt pool, a higher percentage nitrogen was used than for specimen A. A total of 12 laser tracks were produced. . For both Specimens B and C, the laser power was set at 2.8kW and the specimen velocity was 10 mm/s.

The surface roughness of the first, middle and final tracks was measured on the laser treated surfaces by a Talysurf 5 System profile meter. A vertical magnification of either x500 or x1000, together with a cut off of 0.8mm, was used in this work.

After the laser surface processing, the specimen was cut transversely to the direction of the laser track. The track cross-sections were prepared by mounting the specimens in the

bakelite and grinding and polishing by standard metallographic techniques. The polished specimens were chemically etched in a solution of 2gm NH_4.H.HF, 50 ml methanol, and 100 ml H_2O for a period of 1 minute. After etching, the specimens were cleaned by water and methanol and then dried by blasted air. A Nikon Epiphot projection optical microscope and a JEOL JSM 840A scanning electron microscope (SEM) were used for the metallographic studies. The microstructure was characterised using X-ray diffraction (XRD) and X-ray electron photo spectroscopy (XPS), and for these experiments, the specimens were prepared using standard techniques [13,29,54,58].

Microhardness was carried out on the overlapped track cross sections according to the procedures laid down in BS6507-1 1998 and BS 1043-2 1997, with a Mitutoyo MVK-G1 microhardness tester using a load of 100g on metallographically prepared and lightly etched cross-sections. The estimated error was ± 5H_v.

Results

Melt dimensions and microhardness

Fig 1 shows the extent of overlapping and the increase in the melt pool depth from the track 1 to track 7 of specimen A. From the cross section of specimen A shown in Fig2 and the data given in Table 1, it can be seen that the melt pool depth increases progressively from 0.64mm at track1 to 0.80mm at track 3, and then flattens out for tracks 7 and 8 at around 0.94mm. The corresponding data for specimens B and C measured from Figs 3 and 4 are 0.45mm, 0.47 mm (track 6) and 0.47mm, 0.53mm (track7) respectively.

Table 1 also shows that for track 1, the higher energy density of specimen A resulted in an increase of ~ 40% in the cross sectional area (c s a) melted compared with specimen B and 60% compared with specimen C. This percentage increased when the difference between the csa of specimen A at track 7 was compared with that of specimen B ,track 6, and when the c s a' s at tracks 7 for specimens A and C were compared. These changes are mainly due

to the significant increase in melt depth in specimen A as a result of the greater energy, but also the influence of the preheat.

Microhardness maps for the melt pool of specimens A, B and C are shown in Figs 2 to 4. Details of maximum, minimum and average microhardness values are given in Table 2. A comparison between these figures shows clearly that more regions with a hardness >700H_v, which is slightly more than twice that of the base Ti-6Al-4V alloy (325H_v), are found in the laser nitrided specimen A, than in specimens B or C.

In specimen A, Fig 2 shows that higher H_v values were recorded close to the surface for tracks 2 and 7 compared with track 1, which had a much more uniform hardness through the depth of the melt pool. While the part of track1 of specimen A which has not been remelted has only two readings over 700 H_v, that which was overlapped by track 2 has at least five readings over 700 H_v, while track 7, all of which was remelted, has 11 high readings, which continue in track 8. Also the hardness difference between the top and bottom of the melt pool increased from track 1 to track 7.However, a comparison of average hardness data for each track showed only a small spread in the data.

Specimen B shows a similar trend to specimen A, but with a significantly lower hardness close to the surface for track1. The average hardness for track 6 at 660 H_v, was higher than that for specimen A, track 7 at 639H_v.The abnormal value of 1040 H_v was considered to be associated with an agglomeration of undissolved SiC particles close to the surface of track 1.Due to the large number of readings, 35, averaged for track 6, this abnormal reading did not exert an undue influence on the average hardness of 660 H_v.

Specimen C displayed the highest average hardness of the three specimens at 700 H_v. Like specimen B, the spread in hardness within a given track was less than that for specimen A. With the exception of track 1, the differences between the average hardness at the top and bottom of each track in specimen C, were found to be the smallest among

the three specimens. The maximum hardness values in rows 1, 4 and 5 of track 8, were > 720 H_v and the corresponding minimums > 620 H_v. This resulted in the most homogeneous hardness distribution of the three specimens.

Surface roughness

In addition to the surface roughness measurements made on specimens A, B and C, measurements were also made on a Ti-6Al-4V specimen which acted as a standard. The standard specimen had been laser processed to give 13 overlapping tracks under a 100% argon atmosphere [60]. This resulted in a very smooth surface, with a R_a value of <1μm. The surface roughness measurements are collated in Table 3. Specimen A, laser nitrided with a 40%N atmosphere had higher R_a values compared to the argon treated standard specimen and they varied with track position, decreasing from a R_a of 5.1μm for track1 to 2.7μm for track 12. Specimen B showed Ra values similar to the argon treated specimen, with values for tracks 1 and 3 of < 1μm, but the Ra figure for track 6 was closer to 2μm.Combining nitriding and SiC powder laser processing in specimen C increased the surface roughness particularly for tracks 6 and 12, which reached R_a values of ~ 7.5 μm.

Microstructure

Specimen A displayed a thin continuous gold coloured layer at the surface, which was <5μm thick, followed by nearly perpendicular growth of dendrites. Below this, a mixture of small dendrites and needles formed which had a random orientation, Fig 5. From XRD and XPS data, it was found that the main phases present at the surface and to a depth of 300μm, were firstly TiN_x, where x varied between 0.5 and 0.75 depending on track position,1-3 or 6-8, being $TiN_{0.75}$ at the surface, and decreasing with depth. However, TiN_x was not detected below 300μm [58]. Secondly, martensitic α' − Ti, which was confirmed by peaks in the XPS spectra to be a Ti-N solid solution [58].

The surface of specimen B was shiny, reflective and had a white colour. It again showed a thin continuous layer, Fig 6a and c. From XRD studies supported by XPS, three phases, TiC, Ti_5Si_3 and α′-Ti, were identified [29]. For tracks 1-3, XRD showed that the intensity ratios of (TiC (200) + Ti_5Si_3 (300)) / α′-Ti (011), increased from ~ 0.07 at the surface, to 0.16 at a depth of 100 μm, then decreased to 0.25 at a depth of 300 μm below the surface. For the set of tracks 4-6, the same three phases were again formed on the surface, but at depths of 100 and 300 μm below the surface, α′-Ti was the main phase, with some TiC and Ti_5Si_3 present. In this case, the intensity ratio of (TiC (200) + Ti_5Si_3 (300)) / α′-Ti (011) was constant at ~0.14 from the top surface to a depth of 100 μm, and then increased to 0.25 at a depth of 300 μm below the surface [29]. These data suggest that more TiC and Ti_5Si_3 precipitated close to the surface in the later melted tracks due to the effect of the preheat produced by the earlier melted tracks. The pore seen at the melt zone /HAZ interface in Fig 6b will not influence the surface properties.

Several of the features observed in specimens A and B were present in specimen C. The SEM micrograph, Fig 7a, shows that at track 2, a thin continuous film was formed at the surface, whilst below the surface, small dendrites growing nearly perpendicular to the surface were present, as observed in specimen A. The thin surface film was still present at tracks 6/7, Figs 7b and 7c, but below this, a network, consisting of small particles, outlined grains of a size of <10μm, Fig 7b.Dendrites are also observed. At track 7, the surface film was discontinuous, Fig7c, while at depths of 300μm small needles were present, Fig 7d, but no significant dendrites or network particles were found, X-ray spectra showed that the phases present were TiN_x, α′-Ti, a little TiC, and possibly also Ti_5Si_3 and $TiN_{0.3}$. x was in the range 0.65 to 0.8, similar to specimen A. At a depth of

300μm, TiN_x was not found, but the other phases were still detected, and as in the case of specimen A, the presence of a Ti-N solid solution was confirmed [54].

Discussion

Laser surface engineering

A comparison of the effect of different laser conditions on the macro and microstructures and corresponding properties is complex. In addition to the details of the design of the laser, such as $CWCO_2$, Nd-YAG etc, and the laser mode, Gaussian, top-hat etc, there are a number of important parameters which have a major impact on the melt dimensions. These include the input energy density, E, which is expressed as

$$E = q/v \, .r_b \qquad (1)$$

where q = laser power, v= scanning velocity or traverse of the work-piece, and r_b = radius of the laser beam probe. The variation in the input energy density has an effect on the depth of the melt pool, and therefore the volume.

As seen in Table 1, the input energy density, E, calculated from equation 1, associated with specimen A is around 3.6 times greater than that associated with specimens B and C. In the present work, r_b was constant. Other factors which influence the microstructure and hardness include the dimensions of the work-piece, particularly the thickness, the scan pattern adopted, the number of laser tracks melted and the degree of overlapping [61]. Several of these factors determine the preheat, which together with the energy density and the specimen dimensions control the specimen cooling rate and affect the microstructure [60]. Other parameters which are influential include the laser absorptivity, and the Prandtl and Reynolds numbers, all of which are discussed in the literature, for example by Ion [2]. Therefore it is possible to consider the effects of variations in the laser parameters on macro and microstructures and some properties, but far more data needs to be assembled to provide a realistic comparison than has been presented in most publications in the

literature to date. For example, laser melting 13 tracks on a 10mm thick plate of Ti-6Al-4V with q = 2kW,v=5mm/s, r_b = 1mm under an Ar atmosphere, showed that a constant preheat temperature of ~235°C was reached at track 7.With a 20% nitrogen atmosphere using the same conditions, a temperature plateau of 290°C was reached at track 11. Higher temperatures were reached with 5mm thick specimens [60].Therefore it is not surprising that variations in microstructure from the first to the last melted track occurs, although these appear never to be recorded in the literature.

Many papers have discussed the optimization of laser parameters to produce the greatest improvement in properties, such as wear resistance. Morton et al [56] , concluded that 'from the point of view of the economics of the process, the scanning velocity should be as high as possible to reduce costs. However, metallurgical factors in fact limit the scanning velocity because a certain interaction time is required to ensure sufficient homogeneity and to achieve the necessary hardness and melt depth'. The best results for laser processing Ti-6Al-4V plate using a stationary beam were obtained using medium scanning velocities of 15mm/s to 50mm/s and the minimum overlap should be 50% using a stationary beam, otherwise a part of each track will only be molten once [56] .In the present work, using a spinning laser beam, and where economics were not a prime concern, lower scanning velocities were used, usually in the range 3mm/s to 10mm/s, and in agreement with Morton et al [56], a 50% overlap was found to provide the best surface finish, although in earlier work, also using a spinning laser beam, 35% was found to give a satisfactory surface [61].

In practice, the laser processing of surfaces involves the overlapping of many tracks, with a subsequent preheating However, the effect of overlapping and the preheat on the melt dimensions, microstructure and mechanical properties of titanium alloys has received little attention in the open literature [60,62] . Research has been reported for aluminium

alloys on the influence of the overlapped region on corrosion, due to micro-segregation, [63] and changes in phase composition in 321 austenitic stainless steel through overlapping [64], but no similar studies appear to have been reported on titanium alloys.

Melt dimensions and microhardness of specimens A, B and C.

The data in Table 1 show that despite the lower N% in specimen A than specimen C, 20% compared to 40%, the higher energy density in the former produced a greater melt depth for all comparable tracks, regardless of the higher degree of exothermic heat produced by the 40% N atmosphere. The effect of the preheat due to overlapping tracks can gauged by taking the csa of specimen A, track 1 given in Table 1 as reference data for melt dimensions. This shows that the corresponding csa of track 7 is 40% greater, due to the increased depth of melting. Compared with specimen A, the csa of specimen B track 1 is less, due to the significantly lower energy density. However, when this data is compared with that of specimen B track 7, it is apparent that there is again a significant effect of preheat on both the melt depth and csa. A similar influence of preheat is seen for specimen C. Also for specimen C, the addition of the nitrogen atmosphere has resulted in a melt depth which is 14% deeper than specimen B. This increase is considered to result from the exothermic reaction between N and Ti in the formation of TiN.

From the above, it is clear that that when planning which experimental data should be acquired following laser surface engineering, it is not only the laser parameters that should to be considered, but also the track from which the data is obtained, together with the dimensions of the specimens.

Microhardness mapping was undertaken to compare changes in hardness as the overlapping progressed and between specimens. The hardness close to the surface associated with specimens A and C and recorded in Figs 2 and 4, is attributed to the

presence of TiN_x phase distributed in ά-Ti matrix, as the hardness indents do not record the hardness of the TiN_x surface layer only, which is <10μm in thickness.

As in the case of single hardness measurements plotted as a function of depth through the melt pool, given for example in references 8, 57, the hardness decreased from the surface to the bottom of the melt pool. However, unlike some of the published data [6], which showed a very rapid decrease in hardness with distance from the maximum values recorded in the vicinity of the surface, ~10 H_v / μm, in the range 1400 to 500 H_v, the hardness values for specimen A, in Fig 2, show a lower surface hardness which decreases at ~5 H_v / μm, in the range 800-500 H_v. For specimen B, with the exception of the anomalous reading of 1040 for track 6, the hardness values are much more uniform. For track 1, the decrease in hardness from the surface to the reading in row 5 is only 32 H_v over a depth from the surface of 400μm i.e. .08 H_v / μm. It should be noted that H_v ave. was 622 H_v. In the case of specimen C, track 1 row 1 had the highest H_v ave. of 777, but this decreased in track 2 to 621, before increasing at track 8 to 682.Both specimens B and C showed increases in H_v ave. from track 1 to track 6 and 8 respectively. This was considered to be associated with the preheat influencing the microstructure through increasing volume fractions of fine particles precipitated on going from track 1to track 8.

Surface roughness and microstructure

The origin of the surface roughness following the laser radiation of materials surfaces is due to the development of morphologies such as ridges, large scale periodic structures, cones or columns. The surface micro-structuring of titanium in the presence of nitrogen following processing using a Nd-YAG laser has been investigated in detail by György et al [65].They showed that initially a rippled structure developed, which under further irradiation gave way to micro-columns, uniformly distributed on the whole irradiated surface. Nitrogen pressure was also shown to have a significant influence on the surface

morphology. However, 'in argon, smooth flat islands appear, surrounded by a wave-like micro-relief, which evolves with increase in the number of laser pulses towards a smooth surface with polyhedral structures' [65].

The characterization of the surface finish of laser molten layers following CW CO_2 laser processing was considered in terms of roughness and waviness [56]. Roughness, according to Morton et al [56], is due to the amount of surface rippling, which in turn is dependent on the viscosity of the melt. In agreement with this, Xue et al [66] noted that the surface roughness in laser nitrided surfaces is related to the laser process parameters, the nitrogen concentration and the track overlap ratio. To this list, in the case of powder alloying, it is necessary to include the concentration and size of the powder and details of the carrier gas flow. Whilst rippling as a result of laser nitriding is widely reported, it has also been observed after laser boronising Ti 6Al-4V with a preplaced layer of BN [36].

Waviness is a function of the convectional flow of the melt surface and again is influenced by the percent overlap [56]. The use of a spinning rather than a stationary beam had an influence on the surface morphology, which developed cellular –like structures with oval-shaped shiny bands across the tracks [57].

The surface roughness can affect the depth of material required to be removed prior to service. In some cases this may be 40μm. Bell et al [6], found the surface roughness, R_a, after laser nitriding of titanium to be generally <10μm, that is ,smoother than as-ground condition or following shot peening [66], which can show an R_a value of up to 15μm [67] .These data compare with an as- machined roughness of Ti-6Al-4V which can vary widely from 1.4μm [68, 69] to 5μm, depending on the tools and machining parameters [70] . Table 3 gives details of R_a values for specimens A, B and C while Table 4 collates data from previous work [60, 61]. The peak- to- valley height was approximately four times R_a,

which gives data in the range 11 to 29μm. Table 4 shows that for a constant input energy, the R_a value increases as the nitrogen /argon ratio decreases

It can be seen that laser nitriding using 100% N, gave the smoothest surface for both CPTi and Ti-6Al-4V alloys. Decreasing the N% to 60%, resulted in an increase in R_a to 8.6μm which subsequently decreased at 80%N to 5.1μm, when comparison was made with single track R_a data with that found in track 1 of the overlapped specimens. This data compares well with that of Xue et al [66] who found that R_a values of 10.4μm for laser processing Ti-6Al-4V in 70%N30%Ar, reduced to 3.6μm when using 100%N. In the case of CPTi, remelting the 80%N track was shown by Xin et al [61] to decrease R_a to 3.6μm. It is interesting to note that the R_a value varies with track number. With specimen A, R_a decreases with increasing track number, while with specimens B and C, the roughness increased as the track number increased.

Table 2 shows that laser processing Ti-6Al-4V following preplacing of SiC powder produces a very smooth surface, which shows an increase in R_a from of 0.94μm to 1.8μm from track 1 to track 6, but still significantly smaller than any other values collated in this work. However, combining nitriding with powder placement resulted in a marked deterioration in the surface smoothness, with the R_a values again increasing with track number from 4.4μm for track 1 to >7μm for tracks 6 and 12.These were the highest values recorded in the work, but still fall within the limits given by Bell et al [6].

Microstructural characterisation was related to the processing, hardness and roughness data. For the laser nitrided Specimen A, no cracking was observed following processing with a dilute nitrogen atmosphere of 20%N- 80% argon. Previous studies by the present authors have used both X-ray diffraction (XRD) and X-ray photoelectron spectroscopy (XPS) to characterise titanium nitride phases in a Ti-6Al-4V alloy produced by laser nitriding [58, 59]. Single phase δ TiN has an NaCl type fcc structure is more accurately

expressed as TiN_x, as it and can have a wide range of homogeneity from~ 30 to 55 atomic percent nitrogen. In the transition elements, the cubic nitrides can exist in a wide range of non-stoichiometry, and TiN_X can be obtained with $0.5 \leq x \leq 1.1$ [29]. The values of x have been shown to depend on the percentage N in the nitriding atmosphere. With 100%N, x has been estimated to be close to 1, with 80%N, x =0.8 [58], while when 20%N is employed, x decreased to 0.75 [58].

The XPS spectra obtained from different depths in the melt zone, indicate that the quantity of TiN_x precipitates decreased with increasing depth from the surface. Only a small quantity was present at 100μm, while none was detected below 300μm from the surface. At the surface, x was about 0.75 [58]. These results imply that the faster cooling rate resulting from the lower power input of the spinning beam allows the diffusion of nitrogen in the top surface, but not below 300μm from the surface, to a concentration within XRD limits of detection [58]. Some undissolved SiC powder was recorded at the edges of tracks 1 and 6 in specimen B, as were pores at the bottom of tracks 5 and 6 [29]. Pores were also observed in specimen C. Sun et al [44,45] used a CO_2 laser on a 20mm thick Ti-6Al-4V alloy and overlapped the tracks produced by a 6mm laser beam to produce a clad surface from a 1mm depth of NiCrBSi particles in a size range of 50-100μm . This resulted in a clad zone of 1mm thick, having a hardness of $1000H_v$, which decreased to 600 H_v in the middle of the thin dilution zone. The work made no mention of cracking or porosity, or of a changing microhardness profile depending on the track where the microhardness test was made. This is true for all the references given to other work in this paper.

Surface engineering using laser nitriding

Laser nitriding with a 100% nitrogen atmosphere was used in most of the early work in laser surface engineering of titanium alloys, and produced a thin layer of TiN, about 5-

10μm thickness The hardness recorded closest to the surface was 1200-2000H_v ,[4-8,14,20, 56,57]. However, cracking was often observed [6, 8, 20, 56, 57] .Morton et al [56] found that when laser nitriding produced a surface with a hardness >600H_v, it was only possible to avoid cracks by preheating prior to nitriding, which reduced the cooling rate on solidification. An alternative method of alleviating this problem is the use of dilute nitrogen atmospheres, usually in the form of an argon-nitrogen mixture, together with lower nitrogen flow rates [9, 71]. This was found to reduce significantly or eliminate cracking, but at the expense of a decrease in surface hardness, for example using a 50%N50%Ar atmosphere, a reduction to ~800H_v[66]. The variation of hardness of TiN_x as a function of N/Ti ratio was shown by Sproul et al [72] for sputtered coatings, to have a narrow range between 3140 and 3400 $Kgmm^{-2}$, the latter figure also given by Perry et al [73].On the other hand, Munteau and Vaz [74] examining sputtered TiN_x films found that the hardness remained constant with a value about 2000 $Kgmm^{-2}$ within the range 45-55at% N. This variation has been explained by Perry et al [75] as due to an indentation size effect, the higher figure associated with the hardness nearer to the surface. To date it has not been possible to find hardness data related to the stoichiometry of bulk TiN_x, over a wide x range.

Below the surface, the hardness normally decreases rapidly, due to the thin TiN layer, <10μm, being replaced by TiN dendrites in an α'Ti-N solid solution matrix, Fig 5. Closer to the melt zone- HAZ boundary, only the α'Ti-N solid solution is present, and this is reflected in the level of the hardness. While the detailed effect of TiN_x stoichiometry on hardness is not known, reducing the N:Ar ratio to produce dilute nitrogen atmospheres during laser nitriding, reduces x, and also initially results in an increase in surface roughness, to around 3:7 || N:Ar. Laser processing in 100% argon or under a vacuum gives R_a values lower than the 100% N surfaces. The R_a value for specimen A processed

with 20%N, Table 3, decreased from track 1 to track 7 and also had the greatest melt depths which increased with track number. At the same time, the preheat increased as the track number increased, and the total heat was additionally influenced by the exothermic reaction associated with the formation of TiN.

Surface engineering using laser powder alloying

In much of the reported research which has used powder alloying in the laser surface processing treatment, a layer of 0.3 to 1.5 mm of powder or slurry was placed on the surface of the substrate, prior to laser melting [25, 26 ,29, 52, 55] .Unlike laser nitriding, where the reaction between the gas and surface occurs as soon as the top of the work-piece approaches its melting point, in laser powder alloying, due to the higher melting temperature of the powder than of the titanium alloy, the heat generated by the laser has to penetrate the powder before melting the substrate below to form the melt pool. The aim is then to dissolve the powder in the molten layer formed from the substrate. However, the laser processing conditions have to be carefully set to provide both a sufficient level of heat and allow time for dissolution of the powder particles. In some cases the aim was to completely dissolve the powder and precipitate new phases [26-29], while in other work, the aim was to partially dissolve the powders, forming an intermetallic layer to provide a strong bond between the powder and the substrate, but still leaving a sufficiently large powder size to enhance the tribological properties of the surface engineered layer[16-19].

Previous work was undertaken using alloying powders which were derived from a number of sources. For example, Inoue [67] discovered a series of amorphous alloys with a high glass forming ability (GFA) and much lower critical cooling rates in the Mg-, Zr-, Fe-, Pd-, Ti- and Ni based alloy systems. The Zr- based amorphous alloy with the widest supercooled liquid region reported previously, has an extremely high glass-forming

ability. It was considered that these alloy systems with high GFA's opened up bright prospects for laser cladding of amorphous coatings with a high thickness (>1mm)and a large area. Wang et al [47] have applied this idea of synthesizing amorphous layers on crystalline substrates to laser processing CPTi in single passes, using Zr based alloy powders and obtained hardness values which increased from a surface value of 600HK to 1000HK at 0.3-0.5mm depth. No cracks were found. Another approach, with the aim of increasing the matrix hardness, has been to change the matrix crystal structure from hcp to bcc, by alloying Ti-6Al-4V with Mo [25].In practice, the increase in hardness was only from 363H_v of the Ti-6Al-4V alloy to 380H_v, but when a 20%Mo+80%WC powder mix was incorporated into the melt pool, the hardness was increased to ~600H_v. A significant improvement in wear resistance compared with the untreated alloy was recorded [25]. Higher surface hardness values to > 800Hv retained to a depth of 400μm were obtained following laser boronising single tracks with preplaced BN [36].

In the present work, the hcp α-Ti matrix has been retained, but the matrix was strengthened by dispersion hardening [77]. It has been shown that when SiC particles dissolve in a Ti alloy, eutectic Ti_5Si_3 can precipitate, giving improved hardness to the melt pool compared with the parent alloy [21,27-29,31]. It has also been shown that significant improvements in tribological properties are brought about by laser alloying to precipitate Ti_5Si_3 [24].Wang and Liu[46] extended this approach to study the laser alloying with a mixture of Ti_5Si_3+ $NiTi_2$ powders. In addition to the improvement in tribological properties through alloying with Si, it is known that Si additions to Ti alloys depress the liquid/ liquid +β transition temperature, thereby extending the liquid phase to lower temperatures [78]. For example, an addition of 10 A/o Si to Ti lowers the solidification temperature from1670°C to ~1480°C, while a 15 A/o Si addition retains the liquid phase to1330°C [78]. Using this approach, by alloying to increase the Si content of Ti alloys and

provide a longer so liquification temperature range, it was possible to avoid solidification cracking [27, 28]. In the present work, llaser surface alloying Ti-6Al-4V with preplaced SiC produced significantly less melt depth and surface hardness than nitriding. The microstructure was more homogeneous than for specimen A. The surface of specimen B showed a thin continuous layer, Fig 6a and c. Three phases, TiC, Ti_5Si_3 and α'-Ti, were identified [29] and seen in Fig 6a, where Ti_5Si_3 is at boundaries of the α'-Ti grains, while TiC is present within the grains as small spherical particles. The intensity ratios of (TiC (200) + Ti_5Si_3 (300)) / α'-Ti (011), varied both with melt pool depth and track number. The data suggested that more TiC and Ti_5Si_3 precipitated close to the surface in the later melted tracks due to the effect of the preheat produced by the earlier melted tracks. The average hardness for those tracks measured was similar, but the lowest for the three specimens in the study. However, specimen B produced the smoothest surfaces, with $R_a <$ 2 μm.

Surface engineering using laser nitriding and powder alloying

The combination of nitriding with powder alloying to obtain the advantages of both processes does not appear to attracted attention other than by the present Group where it has been explored in several systems: nitrogen with SiC [24, 28, 29,52,53,55] with TiN[24], with ZrC [24] and with ZrN [24].ZrN powders are attractive because sputtered ZrN coatings are known to have a hardness of 4840H_v compared with 3140-3400H_v for TiN [72] and 2400-2800H_v.for bulk SiC [79].However,caution must be exercised in comparing the hardness of sputtered coatings with those from bulk material. For example, Vaz et al [80] quotes values of 8GPa (~800H_v) for the hardness of CTi sputtered films, compared with a bulk hardness of ~200H_v. Initially, 6μm SiC was preplaced on CPTi (IMI 115) and the influence of 100%N and 80%N/20%He was explored after melting single tracks [52]. No cracking was observed in vertical cross sections through the laser track or on the surfaces.

With the 100%N +SiC, microhardness values of 1000H_v close to the surface were retained to100μm depth, followed by a plateau at ~600H_v retained to 1mm depth [52]. By reducing the average size of SiC to 3μm, hardness values over 2000H_v were found and hardness values over 1000 H_v were obtained at 1mm depth, in crack- free material [55]. Laser melting single tracks on 3.8mm thick Ti-6Al-4V using 100% N with 6μm SiC particles, hardness values >1000H_v were obtained and retained to a depth of 500μm in the crack free state [28]. In general most of these hardness values were lower than the highest values recorded in specimens processed by nitriding alone but those invariably contained cracks. Laser processed Ti-6Al-4V alloys were usually more prone to cracking than CPTi [28, 52, 55], which resulted in the use of even more dilute nitrogen atmospheres. Nitriding Ti-6Al-4V alloys with preplaced powders of TiN, ZrC or ZrN was less successful than using SiC, even with atmospheres 40%N+60%Ar. Undissolved particles, a greater tendency to cracking and lower hardness profiles were observed [24]. The combination of nitriding and powder alloying with SiC gave the highest average hardness of the three specimens, A, B and C. Also for specimen C, the addition of the nitrogen atmosphere has resulted in a melt depth which is 14% deeper than specimen B. This increase is considered to result from the exothermic reaction between N and Ti in the formation of TiN. The melt depth increased with track number, and whilst that at track 7 was greater than that at track 6 of specimen B, it was, as expected, less than those recorded for specimen A which was processed with a significantly energy density. A thin continuous film was formed at the surface, whilst below the surface, small dendrites growing nearly perpendicular to the surface were present, Fig 7 a and 7b, and also observed in specimen A. The main phases detected were $TiN_{0.75}$, a little TiC, α′-Ti-N solid solution and possibly also Ti_5Si_3 and $TiN_{0.3}$. At a depth of 300μm, $TiN_{0.75}$ was not found, but the other phases were still detected. The R_a values were the highest found in

the study, up to 8.6μm, but less than values normally associated with the as-ground condition, which can be up to 15μm. Compared with specimens A and C , specimen B was smoother for all tracks, while the combination of nitriding and SiC preplacement, gives the highest R_a values in these experiments.

Conclusions

In the present work, three approaches have been compared for undertaking the surface engineering of a Ti-6Al-4V (IMI-318) alloy using a $CWCO_2$ laser with a spinning beam to process an area of the surface. These were (a) nitriding (b) preplacing 6μm SiC powder or (c) a combination of nitriding and preplaced SiC powder alloying. At least six laser tracks were overlapped by ~50% to process a minimum width of 12 mm. The melt track dimensions, microstucture, hardness and surface roughness were determined and where possible, compared with data presented in a wide range of papers reviewed from the published literature.

It was found that:

1) the preheat generated due to the overlapping influenced the individual track dimensions, microstructure and properties, which were also affected by the laser energy density and the nitrogen concentration in the nitriding atmosphere used in processing specimens A and C.

2) in the present work only specimen C at track 8 contained a crack, but some undissolved SiC powder was recorded at the edges of tracks 1 and 6 in specimen B as were pores at the bottom of tracks 5 and 6.A number of pores were also observed at the melt zone –HAZ interface in specimen C.

3) the microhardness maps allowed details of the variation in hardness with both melt depth and track number to be determined. This is the first time that this method has been followed and does not appear to feature in any of the published literature reviewed in the present paper. The most homogeneous hardness distribution and the highest average hardness was found in specimen C.

4) laser alloying with preplaced SiC powder, specimen B, was shown to produce the smoothest surfaces, with R_a values <2μm, while combining nitriding with powder alloying, specimen C, gave the highest R_a, value, 8.6 μm. However, this was still an improvement on some R_a, values of as ground surfaces.

It is recommended that when multi-track laser specimens are characterised, the details of the microstructure and microhardness are related to a specific track, so that the influence of preheat from previous tracks is apparent. This procedure has rarely been followed in the published literature.

Acknowledgements

MSS gratefully acknowledges SIRIM Berhad and the Malaysian Government for the financial support in this work. The contributions of Dr. Burdett for help of X-ray diffraction analysis Dr. C.Hu with the preparation of the laser specimens are also acknowledged and the advice of Professor D. Gorman.

References

1 ASM Handbook, Vol. 18, Friction, Lubrication and Wear Technology, Metals Park, OH, 1992,p32.

2 Laser Processing of Engineering Materials, J. C. Ion, , Elsevier, Oxford, U.K. 2005, pp261-326.

3 Y.S. Tian, C.Z. Chen, S.T. Li and Q.H. Huo, Appl. Surf. Sci., 2005, **31,** 177-184.

4 S. Katayama, A. Matsunawa, A. Morimoto, S. Ishimoto, Y Arata, Proceedings of the Fifth International Conference on Applied Laser Electro-Optics, 127-134, 1983, Laser Institute of America.

5 A Walker, J Folkes, W.M Steen and D.R.F West, J. Surf. Eng. 1985, **1**, 23-29.

6. T. Bell, H.W. Bergmann, J, Lanagan, P.H Morton and A.M. Staines, J. Surf. Eng. 1985, **2**, 133-143.

7 H.S.Ubhi, T.N.Baker, P.Holdway and A.W.Bowen, (eds P. Lacombe, R.Tricot , G.Berangei), Proc.Sixth World Conf. On Titanium, 1988, 1687-1692,part 1, Les Editions de Physique, Les Ulis,France,

8 S.Mridha and T.N Baker, Mat. Sci. and Eng., 1991, **A142**, 115-124

9 S. Mridha and T.N.Baker, Mat. Sci. and Eng., 1994, **A188,** 229-239

10 V.M.Weerasinghe, D.R.F.T.West and J.de Damdorenea, J.Mat.Proc.Tech. 1996, **58**, 79-86.

11 P.Laurens, H.L.'Enfant, M.C.Sainte Catherine, J.J.Bléchet and J.Amouroux, Thin Solid Films1997, **293**, 220-226.

12 H.L.'Enfant, P.Laurens, M.C.Sainte Catherine, T.Dubois and J.Amouroux, Surf. Coat. Technol. 1997 **6**,169-175.

13 C. Hu, H. Xin, L.M. Watson and T.N. Baker, Acta mater. 1997, **45**, 4311-4322.

14 S. Ettaqi, V.Hays, J.J.Hantzpergue, G.Saindrenan and J.C.Remy, Surf.Coat.Tech. 1998, **100-101**, 428-432.

15 Y.Fou, and A.W.Batchelor, Wear, 1998, **214**, 83-90.

16 A.I.P. Nwobu, R.D Rawlings and D.R.F West, Acta mater**.** 1999, **47,** 631-643.

17 J.D.Ayers, R.T.Schaffer and W.P.Robey J.Met. 1981, **33,** 19-23

18 J.D Ayers and R.N.Bolster, Wear, 1984, **93,** 193-205.

19 J. H. Abboud and D. R. F. West, Mat.Sci.Tech. 1989, **5**, 725-72.

20 K.P.Cooper and P.Slebodnick, J.Laser Applic. 1989, **1**, 21-29.

21 A.B Kloosterman, B.J. Kool, and J. Th. M De Hosson, Acta mater**.** 1998, **46**, 6205-6217.

22 B.J. Kool, M. Kabel, A.B. Kloosterman, and J.Th.M. De Hosson, Acta mater**,**1999, **47**, 3105-3116.

23 Y. T..Pei, V.Ocelik, and J.Th.M.De Hosson, Acta mater**,** 2002, **50**, 2035-2051.

24 C. Hu, H.Xin and T.N Baker, in M.L Scott, (Ed.), Proceedings of the Eleventh International. Conference on Composite Materials, Metal Matrix Composite and Physical Properties, Woodhead Publishing, Abington, UK, 1997,**Vol.3**, 80-89.

25 W. Pan, H.C.Man and T.M.Yue, Mat.Sci. Eng. A, 2005, **A390**,144-153.

26 S. Mridha, H.S.Ubhi, P.Holdway, T.N.Baker, A.W.Bowen in R.H.Froes and I.Caplan, (Eds.) Proceedings of the Seventh International Conference on Titanium,

Titanium '92, Science and Technology, 1993, **Vol 3**, p.2641-2648.

27 T.N.Baker, H.Xin, C.Hu, and S.Mridha, Mat. Sci.Technol. 1994, **10**, 536-544.

28 S. Mridha and T.N Baker, J. Mat. Proc.Tech. 1997, **63**, 432-437.

29 M.S.B Selamat, L.M.Watson and T.N.Baker, J. Mat. Proc. Tech., 2003,**142**, 725-737.

30 J.H.Abboud and D.R.F.West, J. Mater.Sci.Lett.., 1990, **9,**308-310

31 J.H.Abboud and D.R.F.West, Mater.Sci.Technol., 1991**,7**,353-356.

32 J.H.Abboud , R.Rawlings and D.R.F.West, , Mater.Sci.Technol., 1994,**10**,414-419.

33. J.H.Abboud , D.R.F.West, R.Rawlings, Mater.Sci.Technol., 1994,**10**,848-953.

34 J.Dutta Majumdar, B.L.Mordike and I.Manna, Surf.Coat.Technol., 2000,**242**, 18-27.

35 A.Mehlmann, S.F.Dirfeld and I.Minkoff, Surf.Coat.Technol. 1990, **42**, 275-281.

36 J.S.Selvan,K.Subramanian,A.K.Nath,H.Kumar,C.Ramachandra and S.P.Ravindranathan, Mater.Sci.Eng.A, 1999, **A260,** 178-187.

37 J.Dutta Majumdar, B.L.Weisheit, B.L.Mordike and I.Manna, Mater.Sci.Eng.A, 1999, **A266**, 123-134.

38 R.L.Sun, D.Z.Yang, L.X.Guo and S.L.Dong, Surf.Coat.Tech.2001, **135,**307-312.

39 R.L.Sun,J.F.Mao and D.Z.Yang, Surf.Coat.Technol.2002, **155,** 203- 207.

40 H.C.Man, S.Zhang, F.T.Cheng and T.M.Yue, Scripta Mater. 2001, **44**, 2801-2807.

41 B.S.Yilbas, M.S.J.Hashmi and S.Z.Shuja, Surf.Coat.Technol. 2001, **140**, 244-250.

42 R.Banerjee, A.Genç, P.C.Collins and H.L.Fraser, Met.Mat.Trans. 2004, **35A**, 2143-2152.

43 P.A. Molian and L.Hualun, Wear, 1989, **130**, 337-352.

44 R.L.Sun, D.Z.Yang, L.X.Guo and S.L.Dong, Surf.Coat.Technol. 2000, **132**, 251-255.

45 R.L.Sun, D.Z.Yang, L.X.Guo and S.L.Dong, Surf.Coat.Technol. 2002, **150**,199- 204.

46 H.M.Wang and Y.F.Liu, Mater.Sci.Eng.2002, **A338**, 126-132.

47 Y.Wang, G.Li, C.Wang, Y.Xia, B.Sandip and C.Dong Surf.Coat.Tech., 2000, **132**, 251-255.

48 B.Courant, J.J.Hantzperque, L.Avril and S.Benayoun, J.Mat.Proc.Tech., 2005, **160**, 374-381.

49 Y.S.Tain, C.Z.Chen, L.X.Chen and Q.H.Huo, Mat.Lett. 2006, **60**, 109-113.

50 Y.S.Tain, C.Z.Chen, L.X.Chen and Q.H.Huo, Scripta Mater. 2006, **54**, 847-852.

51 L.Covelli,F.Pierdominici,I Smurov and S.Tosto, Surf.Coat.Tech.1996, **78,** 196-204.

52 S. Mridha and T.N Baker, Mat. Sci. Technol., 1996, **12**, 595-602..

53 C. Hu, M.S.B. Selamat, H.S. Ubhi and T.N. Baker, Mat. Sci. Technol., 1998, **14**, 1045-1052.

54 M.S. Selemat, L.M.Watson and T.N.Baker, Surf. Coat. Technol., 2006, **20**, 724-736.

55 S.Mridha and T.N.Baker, J. Mat. Proc. Tech. 2007, **185**, 38-45.

56 P.H.Morton, T.Bell, A.Weisheit, J.Kroll and B.L.Mordike, Surf. Modific. Technol. V, (Ed. T.S.Sudarshan and J.F.Braza), 1992, Inst. Mater., 593-609.

57 S. Mridha and T.N Baker, Proc.Adv.Mater.1994, **4**, 85-94.

58 M.S. Selamat, T.N.Baker and L.M.Watson, J. Mat. Proc. Technol., 2001, **113**, 509-515.

59 H. Xin, L.M.Watson, T.N.Baker, Acta mater. , 1998, **46**, 1949-1961.

60 C.Hu and T.N.Baker, Mater. Sci.Eng.1999, **A265**, 268-275.

61 H. Xin, S. Mridha and T.N Baker, J. Mat.Sci., 1996, **31,**22-30.

62 C. Hu and T.N.Baker, J. Mat. Sci., 1997, **32**, 2821-2826.

63 K.G.Watkins, Z.Liu, M.McMahon, R.Vilar and M.G.S.Ferreira, Mat.Sci. and Eng. 1998, **A252**, 292-300.

64 X.Y.Wang, Z.Liu and P.H.Chong, Thin Solid. Films, 2004,**453-454**,72-75.

65 E.György, A.Pérez del Pino, P.Serrs and J.L.Morenza, Surf.Coat.Technol.,2004, **187,** 245-249.

66 L.Xue, M.Islam, A.K.Koul, M. Bibby and W. Wallace, Adv. Perf. Mater. 1997, **4** 389-408.

67 A.Drechsler, J.Kiese and L.Wagner, 7thInt.Conf. Shot Peening, Inst. Precision Mechanics, 1999 ,145-152, Warsaw, Poland.

68 M.V,Ribeiro,M.R.V.Moreita and J.R.Ferreira, J. Mat. Proc. Tech. 2003, **143-144**, 458-463.

69 R.K.Nalla, L.Altwnberger, U.Noster, G.Y.Liu, B.Scholtes and R.O.Richie, Mat. Sci. Eng., 2003, **355**, 216-230.

70 C. H. Che-Haron, J. Mat. Proc. Tech. 2001, **118**, 231-237.

71H.Xin and T.N.Baker 8th World Conf. on Titanium, Titanium '95, Science and Technology, P.A. Blenkinsop, W.J. Evans and H.M Flower, Inst. Mater., London,1995, 2031-2038.

72 W.D.Sproul, P.J.Rudick and M.E.Graham, Surf. Coat.Technol., 1989, **39-40**,355-363.

73 A.J.Perry, Y.P. Sharkeev, D.E.Geist and S.V.Fortuna, J.Vac.Sci.Technol. A 1999, **17,** 1848-1853

74 D. Munteanu and F.Vaz, J. Optoelect. Adv. Mater., 2006, **8**, 720-725.

75 A J. Perry, S. J. Bull, A. Dommann, M. Michler, B. P. Wood, D. Rafaja and J. N. Matossian, Surf. Coat. Technol., 2000, **140**, 99-108.

76 A.Inoue, Acta mater., 2000**, 48**, 1234-1237.

77 J.W. Martin, Micromechanisms in Particle Hardened Alloys, 1980,Cambridge University Press, Cambridge, UK,

78 ASM Handbook, Vol. 3, Alloy Phase Diagrams, 1992, Metals Park, OH, p2-367

79 R.Morrell, Handbook of Properties of Technical and Engineering Ceramics, Part 1, 1985,HMSO,London, p134.

80 F. Vaza, J. Ferreiraa, E. Ribeiroa, L. Reboutaa, S. Lanceros-Méndeza, J. A. Mendesa, E. Alves b, Ph. Goudeauc, J. P. Rivièrec, F. Ribeirod, I. Moutinhod, K. Pischowe and J. de Rijke, Surf.Coat.Technol., 2005, **191**,317-323.

Appendices

Specimen	Energy Density MJm^{-2}	Track Number	Track Radius mm	Melt Pool Depth mm	Cross Section Area mm^2
A	500	1	1.8	0.64	1.22
		2	1.8	0.69	1.36
		3	2.1	0.80	1.84
		6	2.2	0.92	2.31
		7	2.3	0.96	2.51
B	140	1	2.5	0.45	0.88
		6	2.8	0.47	0.99
C	140	1	1.7	0.47	0.76
		7	2.5	0.53	1.11

Table 1 Energy densities and data on the melt pools of specimens A, B and C

Specimen	Track	Row	Min H_v	Max H_v	H_{vmax}-H_{vmin}	Ave H_v	$H_{v\ row\ a}$-$H_{v\ row\ b}$	Ave of Ave H_v	No. of readings
A	1	1	634	743	109	668			9
	1	6	542	685	143	613	55	640	9
	2	1	627	888	261	709			9
	2	6	572	665	93	622	87	665	5
	7	1	630	808	178	712			12
	7	8	508	649	141	565	147	639	9

Specimen	Track	Row	Min H_v	Max H_v	H_{vmax}-$H_{v\ min}$	Ave H_v	$H_{v\ row\ a}$-$H_{v\ row\ b}$	Ave of Ave H_v	No.
B	1	1	548	644	96	596	1		9
	1	4	579	609		595			8
	1	5	551	585	34	564	32	585	5
	6	1	619	1040		699			20
	6	5	566	694	128	622	77	660	15

Specimen	Track	Row	Min H_v	Max H_v	H_{vmax}-$H_{v\ min}$	Ave H_v	$H_{v\ row\ a}$-$H_{v\ row\ b}$	Ave of Ave H_v	No. of readings
C	1	1	627	1106	479	777			7
	1	4	572	669	97	624	150	700	5
	2	1	616	706	90	649			9
	2	4	582	649	67	615	34		10
	2	5	545	642	97	599	50	621	6
	7	1	508	698	190	636			11
	7	4	569	694	125	622	14		11
	7	5	545	649	104	616	20	625	10
	8	1	642	729	87	687			6
	8	4	623	727	104	680	7		4
	8	5	634	743	109	678	19	682	4

Table 2 Hardness data for specimens A, B and C.

Specimen	Track number	R_a μm
A –Nitrided	1	5.10
(20%N)	6	3.10
	12	2.70
B-SiC preplaced	1	0.94
	3	0.70
	6	1.80
C- Combination	1	4.40
of nitrided (40%N)	6	7.50
and SiC preplacement	12	7.20

Table 3 Surface roughness measurements according to the sequence of track number for specimens A, B and C.

Laser Atmosphere / powder	CPTi R_a μm	Ti- 6Al-4V alloy R_a μm
100% nitrogen	2.7	4.6
80% nitrogen / 20% argon	7.2	5.7
60% nitrogen / 40% argon	5.4	8.6
20% nitrogen / 80% argon		5.1
40% nitrogen / 60% argon +SiC		4.4
(track 1)		
100% argon /SiC (track 1)		0.94
100% argon / SiC (track 3)		0.70
100% argon /SiC (track 6)		1.80

Table 4 Average surface roughness for nitrided CPTi and 318 Ti from ref. 60.61 and selected data from Table 3

Figures

Fig 1

Fig 2.

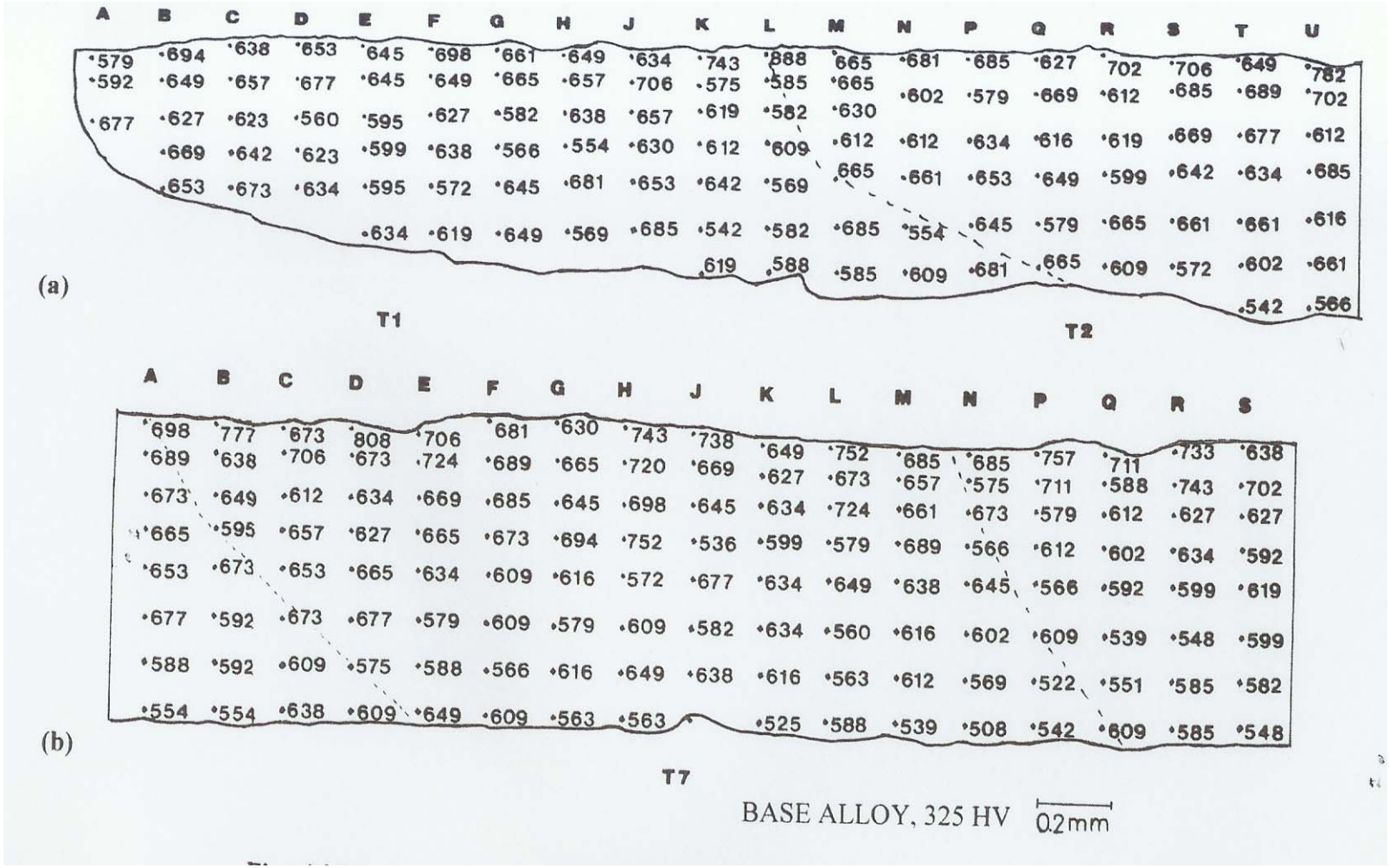
A B C D E F G H J K L M N P Q R S T U
(a)
T1
T2
A B C D E F G H J K L M N P Q R S
(b)
T7
BASE ALLOY, 325 HV
0.2mm

Fig 3

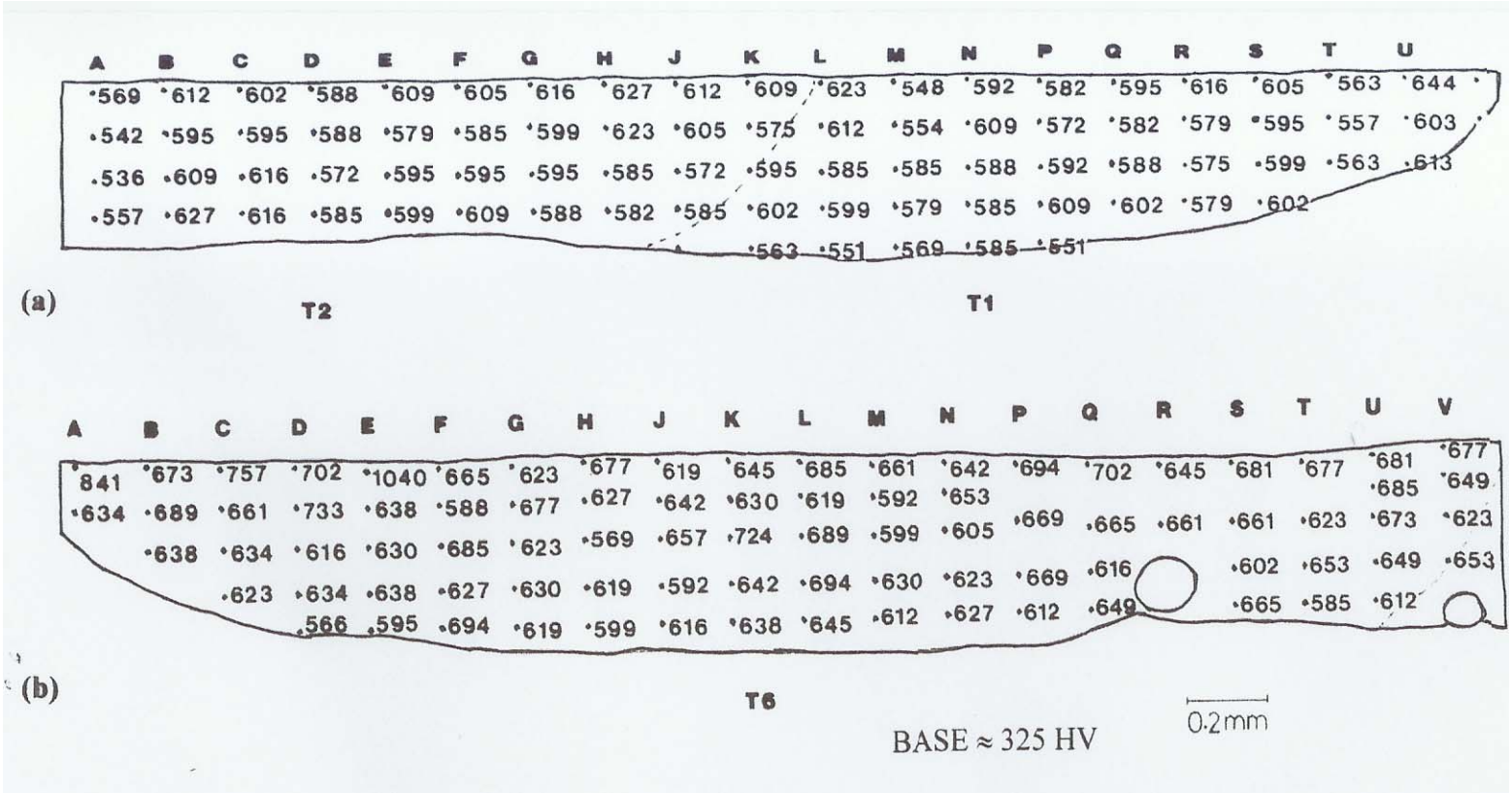
A B C D E F G H J K L M N P Q R S T U
·569 ·612 ·602 ·588 ·609 ·605 ·616 ·627 ·612 ·609 ·623 ·548 ·592 ·582 ·595 ·616 ·605 ·563 ·644
·542 ·595 ·595 ·588 ·579 ·585 ·599 ·623 ·605 ·575 ·612 ·554 ·609 ·572 ·582 ·579 ·595 ·557 ·603
·536 ·609 ·616 ·572 ·595 ·595 ·595 ·585 ·572 ·595 ·585 ·585 ·588 ·592 ·588 ·575 ·599 ·563 ·613
·557 ·627 ·616 ·585 ·599 ·609 ·588 ·582 ·585 ·602 ·599 ·579 ·585 ·609 ·602 ·579 ·602
·563 ·551 ·569 ·585 ·551
(a)
T2
T1
A B C D E F G H J K L M N P Q R S T U V
·841 ·673 ·757 ·702 ·1040 ·665 ·623 ·677 ·619 ·645 ·685 ·661 ·642 ·694 ·702 ·645 ·681 ·677 ·681 ·677
·634 ·689 ·661 ·733 ·638 ·588 ·677 ·627 ·642 ·630 ·619 ·592 ·653 ·685 ·649
·638 ·634 ·616 ·630 ·685 ·623 ·569 ·657 ·724 ·689 ·599 ·605 ·669 ·665 ·661 ·661 ·623 ·673 ·623
·623 ·634 ·638 ·627 ·630 ·619 ·592 ·642 ·694 ·630 ·623 ·669 ·616 ·602 ·653 ·649 ·653
·566 ·595 ·694 ·619 ·599 ·616 ·638 ·645 ·612 ·627 ·612 ·649 ·665 ·585 ·612
(b)
T6
BASE ≈ 325 HV
0.2mm

Fig 4

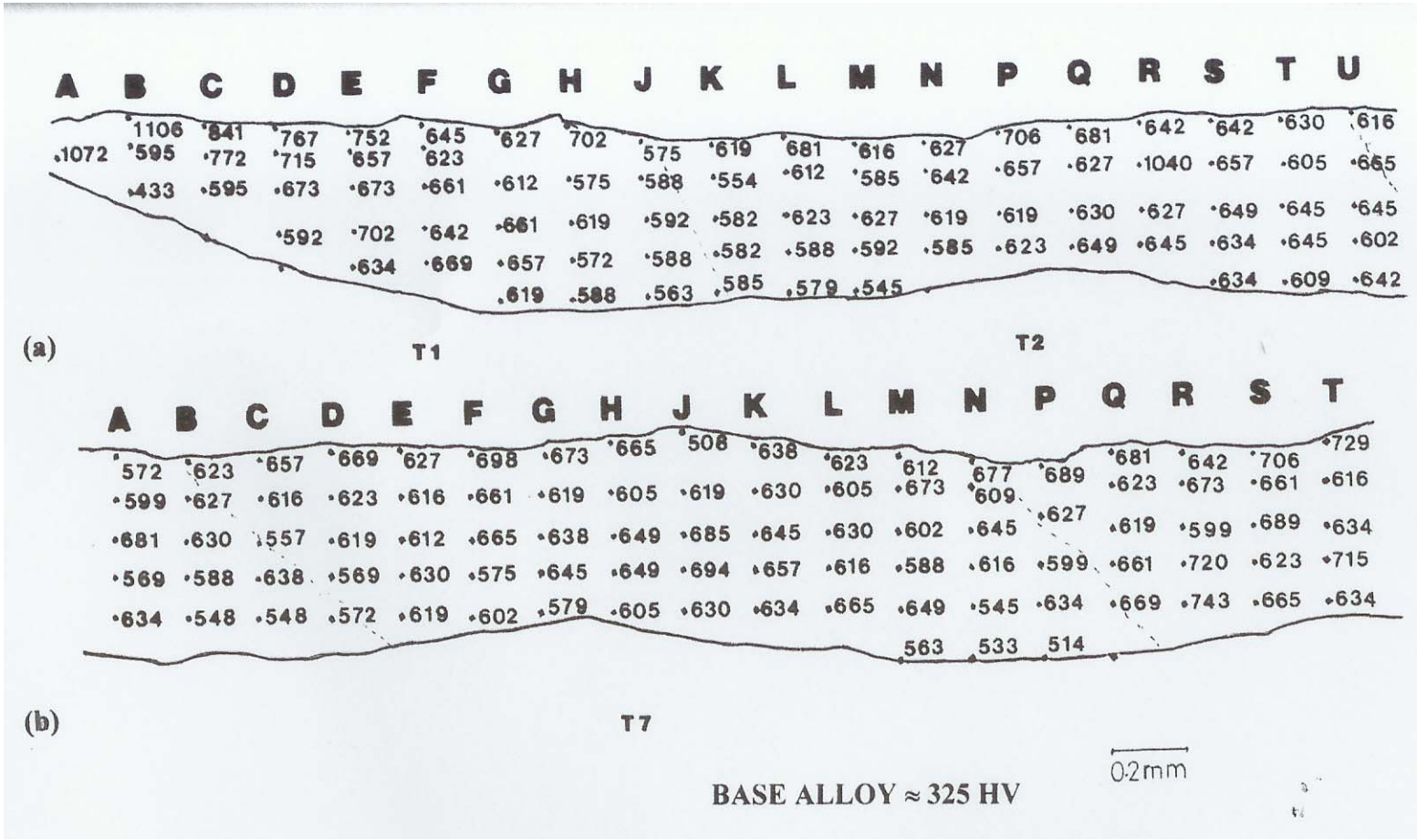
A B C D E F G H J K L M N P Q R S T U
1106 841 767 752 645 627 702 575 619 681 616 627 706 681 642 642 630 616
1072 595 772 715 657 623 612 588 554 612 585 642 657 627 1040 657 605 665
433 595 673 673 661 612 575 588 554 612 585 642 657 627 1040 657 605 665
592 702 642 661 619 592 582 623 627 619 619 630 627 649 645 645
634 669 657 572 588 582 588 592 585 623 649 645 634 645 602
619 588 563 585 579 545 634 609 642
(a)
T1
T2
A B C D E F G H J K L M N P Q R S T
572 623 657 669 627 698 673 665 508 638 623 612 677 689 681 642 706 729
599 627 616 623 616 661 619 605 619 630 605 673 609 627 623 673 661 616
681 630 557 619 612 665 638 649 685 645 630 602 645 619 599 689 634
569 588 638 569 630 575 645 649 694 657 616 588 616 599 661 720 623 715
634 548 548 572 619 602 579 605 630 634 665 649 545 634 669 743 665 634
563 533 514
(b)
T7
0·2mm
BASE ALLOY ≈ 325 HV

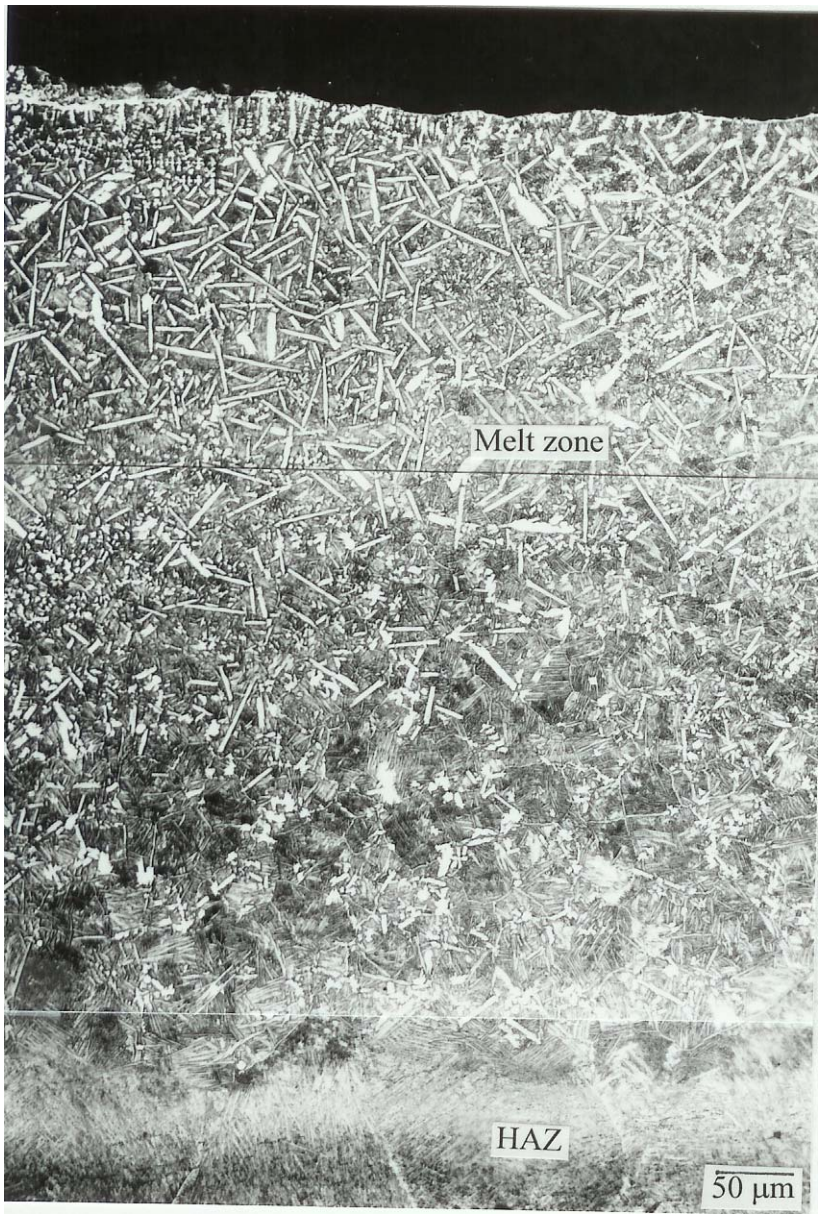

Fig 5

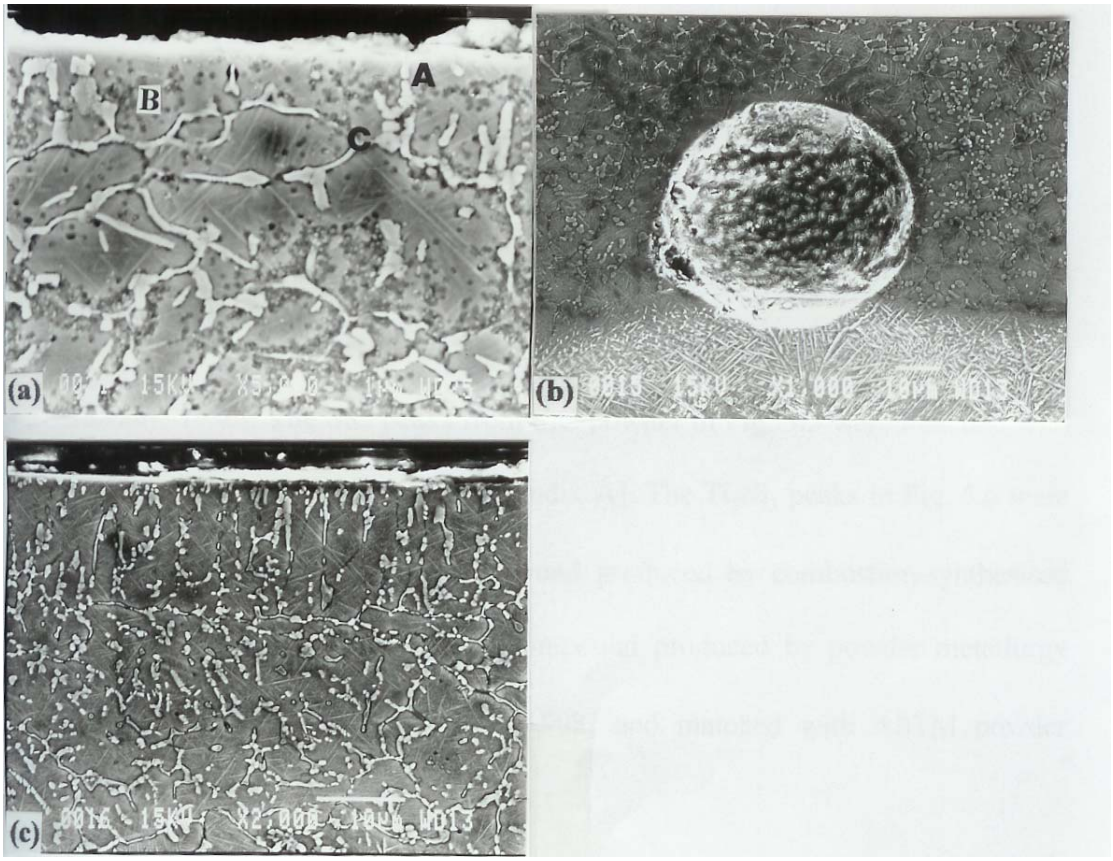

Fig 6